

ATM: IMPROVING MODEL MERGING BY ALTERNATING TUNING AND MERGING

Luca Zhou* Daniele Solombrino* Donato Crisostomi Maria Sofia Bucarelli
Fabrizio Silvestri Emanuele Rodolà

Sapienza University of Rome

zhou.2135393@studenti.uniroma1.it
{solombrino, crisostomi, rodola}@di.uniroma1.it
{bucarelli, silvestri}@diag.uniroma1.it

ABSTRACT

Model merging has recently emerged as a cost-efficient paradigm for multi-task learning. Among current approaches, task arithmetic (Ilharco et al., 2022) stands out for its simplicity and effectiveness. In this paper, we motivate the effectiveness of task vectors by linking them to multi-task gradients. We show that in a single-epoch scenario, task vectors are mathematically equivalent to the gradients obtained via gradient descent in a multi-task setting, and still approximate these gradients in subsequent epochs. Furthermore, we show that task vectors perform optimally when equality is maintained, and their effectiveness is largely driven by the first epoch’s gradient. Building on this insight, we propose viewing model merging as a single step in an iterative process that Alternates between Tuning and Merging (ATM). This method acts as a bridge between model merging and multi-task gradient descent, achieving state-of-the-art results with the same data and computational requirements. We extensively evaluate ATM across diverse settings, achieving up to 20% higher accuracy in computer vision and NLP tasks, compared to the best baselines. Finally, we provide both empirical and theoretical support for its effectiveness, demonstrating increased orthogonality between task vectors and proving that ATM minimizes an upper bound on the loss obtained by jointly finetuning all tasks.

1 INTRODUCTION

The pretrain-and-finetune paradigm has become the standard for many deep learning tasks, where a model pretrained on large-scale, unlabeled data is adapted to a specific downstream task with minimal tuning. However, when working with multiple tasks, a major drawback is the need to store separate finetuned models for each task. Model merging addresses this challenge by combining task-specific models into a single model capable of handling all tasks. This significantly reduces storage costs, as the unified model’s size remains comparable to that of a single-task model, regardless of the number of tasks. Among numerous model merging methods, *task arithmetic* (Ilharco et al., 2022) stands out for its simplicity and effectiveness. Given a pretrained model θ_0 and a model θ_i finetuned on task t_i , the *task vector* $\tau_i = \theta_i - \theta_0$ is defined as the difference between the finetuned and pretrained weights. For multi-task learning with n tasks, task arithmetic sums the n task vectors, scales the sum with a coefficient α , and adds the resulting vector back to the pretrained model.

In this paper, we explain the effectiveness of task arithmetic by linking task vectors to the gradients of the average loss across all tasks. We start from a simple observation: when a model is finetuned for a single epoch using gradient descent (GD), the corresponding task vector is the additive inverse of the loss gradient, scaled by the learning rate. Similarly, the multi-task vector, obtained by summing individual task vectors, is equivalent to the additive inverse of the *average* loss gradient. Thus, task addition is analogous to performing a GD step on the sum of the average task losses.

When finetuning spans multiple epochs, this equality becomes an approximation, with an error dependent on the learning rate. Despite the single-epoch assumption not always holding in practice,

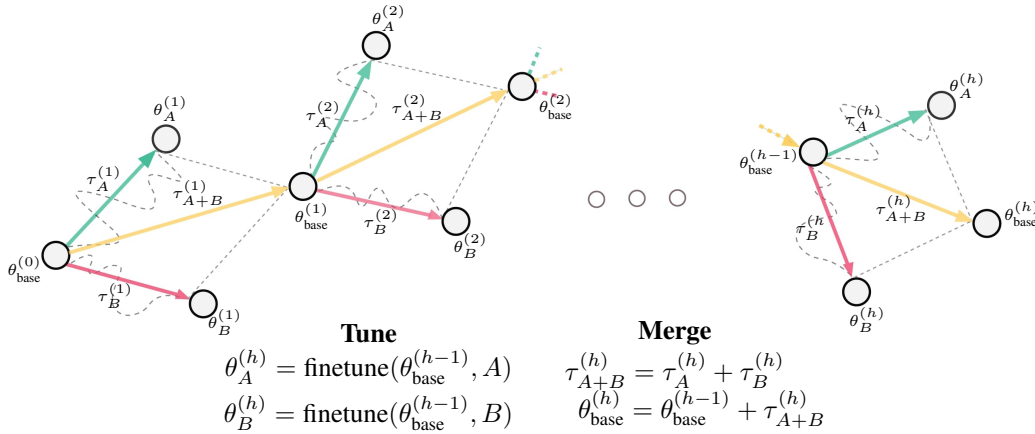


Figure 1: The ATM method, illustrated up to iteration h with two tasks (A and B). In each iteration, the **Tune** step finetunes the pretrained model $\theta_{\text{base}}^{(0)}$ separately on both tasks, and the **Merge** step aggregates the task vectors and applies the resulting multi-task vector to the base model. This process repeats, with each iteration using the updated model as the new base, continuing until a stopping condition is met. We observe increased task vector orthogonality as ATM iterations progress.

the gradient analogy still sheds light on why task vectors are effective. In fact, we reveal that the first epoch often contributes the most to the overall gradient norm during finetuning. Even when this is not the case, subsequent gradients tend to align with the first, confirming that the initial direction predominantly dictates the task vector’s effectiveness.

In this view, aggregation and merging in task arithmetic correspond to a noisy GD step when finetuning on the combined tasks, using the sum of the average losses as the objective. In practice, this implies that the one-step nature of these techniques likely leads to overshooting the multi-task minimum, as they effectively perform GD on a multi-task dataset with a single, noisy step. The scaling factor optimized over the validation set essentially acts as the learning rate in this process.

Contribution Building on these insights, we address the limitations of one-step task vector methods with Alternating Tuning and Merging (ATM) – a novel framework that iteratively alternates between finetuning and merging. This approach generalizes task arithmetic, allowing for a more gradual and refined integration of task-specific knowledge.

Given a compute budget of b epochs per task, traditional methods allocate b epochs to a single finetuning pass. In contrast, ATM distributes this budget across k iterations, performing $\frac{b}{k}$ epochs of finetuning in each iteration, followed by task vector aggregation. The unified model from each iteration serves as the starting point for the next, and after k iterations, the final unified model is deployed and evaluated. Notably, ATM is agnostic to the merging framework, allowing the integration of any interference-resolution techniques during the merge step to enhance performance. Overall, ATM significantly reduces time overhead compared to current baselines; extensive experiments in vision and NLP demonstrate its state-of-the-art results without hyperparameter tuning.

All code, experiment configurations, and checkpoints are available for reproducibility¹. To summarize, our contributions are four-fold:

- We show that, under specific conditions, task vectors are equivalent to or approximate the gradients of the corresponding task losses.
- We point out that existing one-shot merging frameworks often overshoot the multi-task optimum, especially when task vectors have large norms.
- We introduce Alternating Tuning and Merging (ATM), a novel model merging framework that generalizes task arithmetic. Its flexibility allows it to incorporate any interference-resolution method with no additional overhead.

¹<https://github.com/LuckerZOfficial/Alternating-Tuning-and-Merging>

- We empirically demonstrate that ATM increases task vector orthogonality compared to standard methods, and mathematically prove that it reduces the loss of a jointly finetuned multi-task model.

2 RELATED WORK

Mode connectivity and model merging Mode connectivity studies how weights characterize local minima in the loss landscape. Frankle et al. (2020) explored linear mode connectivity in models trained from the same initialization, while Entezari et al. (2022) suggested that all models converge to a shared basin once neuron permutations are resolved. Building on this, permutation-based model merging combines diverse models into a single one, inheriting their capabilities without ensembling overhead. Singh & Jaggi (2020) introduced an optimal-transport weight-matching method, while Git Re-Basin (Ainsworth et al., 2022) proposed three variants acting both on weights and activations, and REPAIR (Jordan et al., 2023) demonstrated significant barrier reduction through activation renormalization. Most recently, Navon et al. (2023) suggested merging models in the embedding space of deep neural networks, while Crisostomi et al. (2024) proposed a cycle-consistent matching procedure for improved merging. When models share the same pretrained initialization, Wortsman et al. (2022) proposed fusing them via a simple average. Jolicoeur-Martineau et al. (2023) proposed to merge models by pushing them towards the population mean to ensure stability. Reg-Mean (Jin et al., 2022) and Fisher-weighted averaging (Matena & Raffel, 2021) fall under the regime of weighted averaging, where the weights are optimized according to some criteria. Daheim et al. (2023) shed light on the positive relation between post-averaging multi-task performance and the gradient mismatch between the constituent models. Finally, Choshen et al. (2022) proposed model merging as a replacement for pretraining; they argue that pretrained checkpoints are not always the optimal starting point for further finetuning, and a model obtained by merging finetuned models can be a better starting point than any of its constituents.

Task vectors Task vector-based merging (Ilharco et al., 2022) finetunes a pretrained model on different tasks to obtain task vectors (differences between finetuned and original checkpoints). Arithmetic operations on these vectors enable forgetting, analogy learning, and multi-task learning. Several works aim to improve task vector merging by reducing task interference (Deep et al., 2024; Wang et al., 2024; Huang et al., 2024). Some methods include sparsifying task vectors or finetuning only lottery tickets (Panda et al., 2024). TIES-merging (Yadav et al., 2023) merges vectors by pruning, selecting a unified sign vector, and merging disjointly, while Model Breadcrumbs (Davari & Belilovsky, 2023) prunes both small and large-magnitude weights. DARE Merging (Yu et al., 2023) randomly masks out a portion of weights and scales up the rest. AdaMerging (Yang et al., 2023) optimizes aggregation coefficients, while Yang et al. (2024) proposed task-specific modules for test-time adaptation. Ortiz-Jimenez et al. (2024) introduced the concept of weight disentanglement and recommended finetuning in the tangent space. In contrast to these one-shot methods, we present an *iterative* model merging approach that progressively refines a base model to achieve improved multi-task performance.

3 TASK VECTORS AS GRADIENTS

In this section, we show that task vectors are tightly related to the loss gradients over the union of the tasks.

Theorem 3.1. *Let $\left\{\theta_t^{(k)}\right\}_{t=1}^{|T|}$ be a set of models obtained by finetuning the base model θ_{base} for k epochs on tasks T using GD with a learning rate η , where finetuning task $t \in T$ minimizes the loss $\bar{L}_t(\theta) = \frac{1}{n_t} \sum_{i=1}^{n_t} \ell(x_i, y_i, \theta)$. Additionally, let $\left\{\tau_t^{(k)}\right\}_{t=1}^{|T|}$ denote the corresponding set of task vectors, with each $\tau_t^{(k)} = \theta_t^{(k)} - \theta_{base}$. Let $\tau_{MT}^{(k)}$ be the multi-task vector $\tau_{MT}^{(k)} = \sum_{t \in T} \tau_t^{(k)}$. Finally, let $\theta_{MT}^{(k)}$ represent the model obtained by minimizing the combined loss $\sum_{i=1}^{|T|} \bar{L}_i$ for k epochs using*

GD with a learning rate of $\alpha\eta$. It holds that

$$\tau_{MT}^{(1)} = -\eta \nabla \sum_{t \in T} \bar{L}_t(\theta_{base}) \quad (1)$$

$$\tau_{MT}^{(k)} = -\eta \sum_{t \in T} \sum_{j=0}^{k-1} \nabla \bar{L}_t(\theta_{MT}^{(j)}) + \frac{\eta^2}{2} C(\{\theta_{MT}^{(j)}\}_{j=1}^{k-2}) + O(\eta^3) \quad (2)$$

with

$$C(\{\theta_{MT}^{(j)}\}_{j=1}^h) = \sum_{t \in T} \sum_{\ell=0}^h \nabla^2 \bar{L}_t(\theta_{MT}^{(\ell)}) \sum_{m=0}^{\ell} \left[\alpha \sum_{t' \neq t, t' \in T} \nabla \bar{L}_{t'}(\theta_{MT}^{(m)}) + (\alpha - 1) \nabla \bar{L}_t(\theta_{MT}^{(m)}) \right] \quad (3)$$

We provide the proof in Appendix A.1. To better appreciate the relationship between a task vector and the gradient computed on the corresponding task dataset, consider the single-task case, where the task vector is exactly the additive inverse of the gradient, scaled by the learning rate η .

Remark 3.1. From Theorem 3.1, it follows that, for a single task t , and after a single finetuning epoch,

$$\tau_t = -\eta \nabla \bar{L}_t(\theta_{base}) \quad (4)$$

where η is the learning rate.

This implies that, under the theorem’s assumptions, adding the task vector to the pretrained model approximates the effect of finetuning the model; the same intuition applies to the multi-task case.

In fact, in Fig. 2 we report evidence that the multi-task model obtained by merging models finetuned for a *single* epoch outperforms the one obtained by merging models finetuned to convergence. In other words, *the optimal merged model is achieved when task arithmetic is exactly a GD step*.

We formalize this through the following corollary.

Corollary 3.1.1. Let $\theta_{TA}^{(k)} = \theta_{base} + \alpha \sum_{t=1}^T \tau_t^{(k)}$ be the model obtained using vanilla task arithmetics. Using the same notation of Theorem 3.1, it holds that

$$\theta_{TA}^{(1)} = \theta_{MT}^{(1)} \quad (5)$$

$$\theta_{TA}^{(k)} = \theta_{MT}^{(k)} + \frac{\eta^2}{2} C(\{\theta_{MT}^{(j)}\}_{j=1}^{k-2}) + O(\eta^3) \text{ for } k > 1 \quad (6)$$

The corollary indicates that for $k > 1$, the multi-task vector still approximates the gradient of a model finetuned for the same number of epochs via GD, with an error on the order of $o(\eta^2)$. Despite the lack of exact equivalence, the effectiveness of task vectors still holds and can be explained by the fact that most of the model’s finetuning trajectory is driven by the gradient from the first epoch.

In Fig. 3a we plot the epoch-wise normalized gradient norm $\frac{\|\nabla_{\theta}^{(k)} L\|}{\sum_{k'=1}^K \|\nabla_{\theta}^{(k')} L\|}$. We observe that the first epoch contributes the most, accounting for up to 70% of the total gradient norms across all epochs. In cases where this is not true, such as with the RESISC45 dataset, we speculate that the direction is still largely determined by the first epoch. As depicted in Fig. 3b, the gradients from the first 5 epochs maintain a high cosine similarity (> 0.8) with the first epoch’s gradient.

It is worth recalling that this analysis does not apply exactly when using SGD instead of GD. However, treating SGD as an approximation to GD preserves the intuition. From this view, reducing task interference corresponds to minimizing conflicting gradients in multi-task learning.

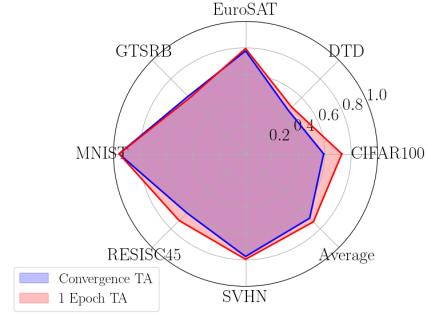
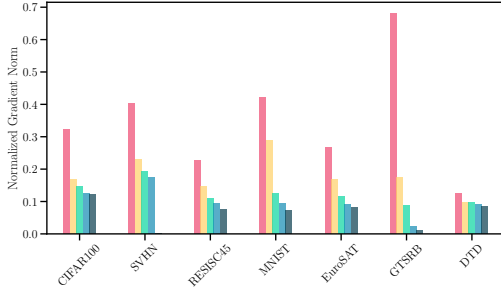
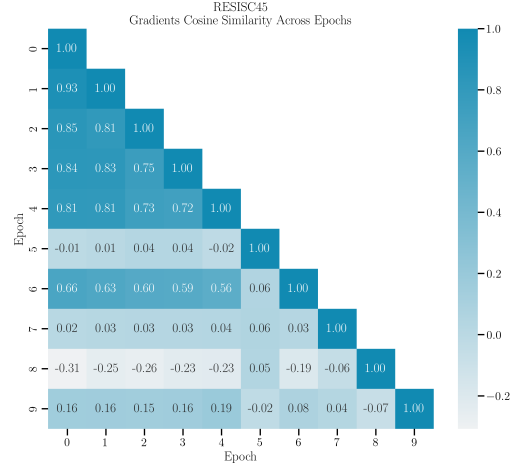


Figure 2: Accuracy of a model merged using task vectors over the task-specific models finetuned for 1 epoch and to convergence.



(a) Normalized gradient norms after 5 epochs of fine-tuning.



(b) Pairwise cosine similarities of the gradients of the first 10 epochs over the RESISC45 dataset.

4 ATM: ALTERNATING TUNING AND MERGING

Building upon the insights of Section 3, we argue that task arithmetic is an approximation to a single GD step over the union of all the tasks. Following this parallel, we advocate taking further update steps iteratively.

The overall framework of ATM is depicted in Fig. 1. Specifically, starting from a pretrained checkpoint as the base model $\theta_{\text{base}}^{(0)}$, we finetune it separately on each task to obtain the first-iteration task vectors $\tau_1^{(1)}, \dots, \tau_{|T|}^{(1)}$. These are then aggregated and added to the base model to form the next-iteration unified model $\theta_{\text{base}}^{(1)}$. The procedure is iterated according to the following equation:

$$\theta_{\text{base}}^{(k+1)} = \theta_{\text{base}}^{(k)} + \frac{\alpha}{|T|} \sum_{t \in T} \tau_t^{(k)} \quad \forall k = 0, \dots, K-1. \quad (7)$$

The k -th iteration task vector for task t is obtained as $\tau_t^{(k)} = \theta_t^{(k)} - \theta_{\text{base}}^{(k)}$, where $\theta_t^{(k)}$ is a model obtained finetuning the k -th iteration base model $\theta_{\text{base}}^{(k)}$ on task t . The total number of iterations K can be predefined or based on a stop condition.

In practice, each iteration of ATM involves finetuning the current base model on all $|T|$ tasks of interest, thereby obtaining $|T|$ task vectors. These task vectors determine the task-specific directions the current base model should follow in order to attain enhanced performance on the corresponding tasks.

The merging step of ATM at a given iteration simply consists of summing the mean current-iteration task vectors to the current base model, although any interference-resolution method in the task vector literature can be integrated. This step is intended to pull the base model closer to the multi-task basin on the loss landscape. Taking the average over T ensures the magnitude of the update remains insensitive to the number of tasks.

Note that after each iteration, the task vectors of the previous iterations can be safely discarded. Therefore, at any stage of ATM, we only store the current base model and one task vector for each of the $|T|$ tasks, incurring no additional memory requirements.

5 UPPER BOUNDING THE MULTI-TASK LOSS

In this section, we explore the relationship between the ATM loss, defined as the mean of average losses over all tasks, and the loss of a model trained jointly on all the datasets. Analogously to Section 3, we conduct this analysis under the assumption that GD, rather than SGD, is used for optimizing the model parameters. This simplifying assumption removes the stochasticity introduced

by random sampling, enabling a more straightforward analysis while still providing valuable insights into the underlying dynamics of the optimization process. With a slight abuse of notation, we denote with t both the task and its corresponding dataset with cardinality n_t . The total number of samples for all tasks is given by $N = \sum_{t \in T} n_t$.

Inspired by Daheim et al. (2023), we define the *target loss* for model merging as $L_{\text{target}}(\theta) = \frac{1}{N} \sum_{i=1}^N \ell(x_i, y_i, \theta)$, which is the loss of a model trained jointly on all the datasets. By Theorem 3.1, when merging occurs after one step of finetuning on each dataset, the ATM update is given by:

$$\theta_{\text{base}}^{(k+1)} = \theta_{\text{base}}^{(k)} + \frac{\alpha}{|T|} \sum_{t \in T} \tau_t^{(k)} = \theta_{\text{base}}^{(k)} - \alpha \eta \nabla \left(\frac{1}{|T|} \sum_{t \in T} \bar{L}_t \right), \quad (8)$$

which corresponds to performing a GD step over the loss $L_{\text{ATM}} = \frac{1}{|T|} \sum_{t \in T} \bar{L}_t$.

Having established that one step of ATM in GD minimizes L_{ATM} , a crucial question arises: under what conditions does minimizing L_{ATM} imply the minimization of L_{target} ? In other words, when can we be certain that optimizing the ATM loss will also minimize the loss associated with training jointly on all datasets?

To answer this question, we first note that L_{ATM} is an unweighted average of the individual dataset losses, while the target loss is a weighted average:

$$L_{\text{target}}(\theta) = \frac{\sum_{t \in T} n_t \bar{L}_t(\theta)}{\sum_{t \in T} n_t}. \quad (9)$$

We now analyze the parameter update from $\theta^{(k)}$ to $\theta^{(k+1)}$. For both ATM and target methods, we denote the change in loss, L_{method} , as $\Delta L_{\text{method}} = L_{\text{method}}(\theta^{(k)}) - L_{\text{method}}(\theta^{(k+1)})$. In the following theorem, we prove that if the drop in ATM loss exceeds a threshold δ , the target loss will also decrease. The value of δ depends on the size of the largest dataset with a decreasing loss and the smallest dataset with an increasing loss. In particular, if the former dataset is larger than the latter, a reduction in ATM loss reduces the target loss. In practice, this is ensured when the loss is reduced on the largest dataset.

Theorem 5.1. *Let $D = \{t \mid \Delta \bar{L}_t > 0\}$ be the set of datasets where the loss decreases after a parameter update, and $I = \{t \mid \Delta \bar{L}_t \leq 0\}$ be the set of datasets where the loss increases or remains unchanged. If the reduction in the ATM loss satisfies $\Delta L_{\text{ATM}} > \delta$, where*

$$\delta = \frac{1}{|T|} \left(1 - \frac{\min_{t \in I} n_t}{\max_{t \in D} n_t} \right) \sum_{t \in I} |\Delta \bar{L}_t|,$$

then the target loss L_{target} will also decrease, i.e., $\Delta L_{\text{target}} > 0$.

We redirect the reader to Appendix A.2 for the formal proof.

Remark 5.1. *If we choose the target loss to be the maximum of the average loss across all datasets $L_{\text{target}} = \max_{t \in T} \bar{L}_t$, by leveraging the equivalence between the L_1 -norm and the max norm, we obtain the bound $L_{\text{target}} \leq T \cdot L_{\text{ATM}}$.*

6 EXPERIMENTS

In this section, we compare ATM against several recent baselines across a number of classification tasks in computer vision and NLP.

6.1 EXPERIMENTAL SETTING

Datasets and Models For computer vision tasks, we test ATM with a ViT-B-16 backbone (Dosovitskiy et al., 2021) and evaluate it on a diverse set of datasets: *CIFAR100* (Krizhevsky et al., 2009), *DTD* (Cimpoi et al., 2014), *EuroSAT* (Helber et al., 2019), *GTSRB* (Houben et al., 2013), *MNIST* (Lecun et al., 1998), *RESISC45* (Cheng et al., 2017), and *SVHN* (Netzer et al., 2011). For NLP tasks, we employ RoBERTa-base (Liu, 2019) and BERT-base-uncased (Devlin et al., 2019), evaluating them on the *GLUE benchmark* (Wang et al., 2019).

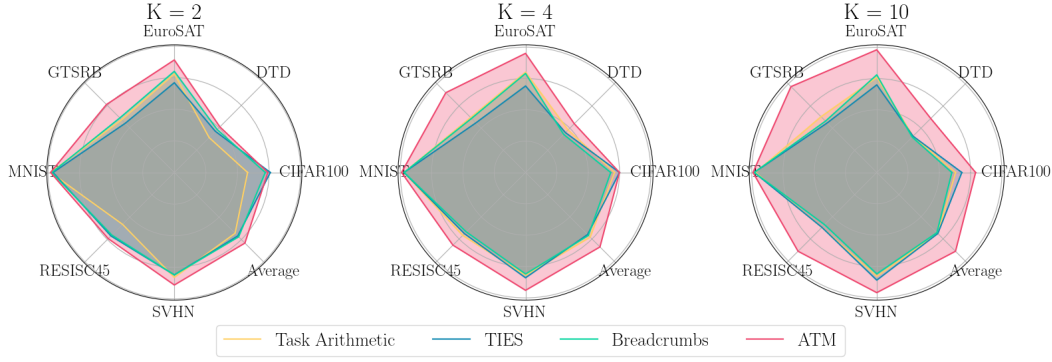


Figure 4: Comparisons as computational budget K varies for ViT-B-16.

Baselines and Metrics To gauge the performance of ATM, we consider several model merging baselines, including task arithmetic (TA) (Ilharco et al., 2022), TIES-merging (Yadav et al., 2023), and model breadcrumbs (Davari & Belilovsky, 2023) for both computer vision and NLP tasks, and DARE merging (Yu et al., 2023) for NLP tasks only. We adhere to the author-recommended hyperparameters, whenever needed or available, in order to ensure fair comparisons across experiments. Specifically, for TIES-merging, we retain the top 15% of weights based on magnitude ranking. For model breadcrumbs, we set $\beta = 0.85$ and $\gamma = 0.993$. For DARE merging, we use a drop rate of 0.9. In all settings, we adopt mean aggregation of task vectors and use a scaling factor of 1 when applying them to the base model.

6.2 IMPACT OF EPOCH DISTRIBUTION ON PERFORMANCE

In this experiment, we first establish a fixed compute budget of 10 finetuning epochs for each task. Then, we seek the optimal distribution of epochs among different numbers of ATM iterations. To exemplify, if 10 epochs are distributed among 5 iterations, then in each iteration a task is finetuned for 2 epochs.

As depicted in Fig. 5, with a fixed compute budget, maximizing iterations while minimizing epochs per iteration yields the best results for ATM. This indicates that more gradual updates to the base model are preferable to abrupt ones. Splitting 10 epochs across 10 iterations achieves the highest average accuracy of 89%, outperforming the 1 iteration of 10 epochs setting (analogous to task arithmetic) by 21%. Based on this, we use the 1 epoch, 10 iterations setting for most subsequent experiments.

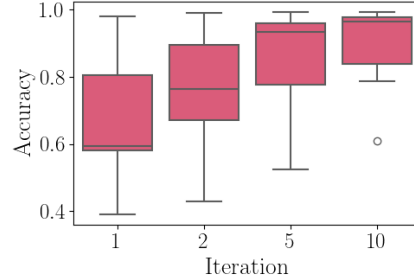


Figure 5: Multi-task accuracy for different budget distributions (ViT-B-16).

6.3 EFFECT OF COMPUTE BUDGET

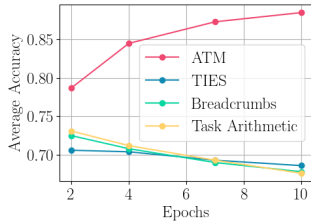


Figure 6: Average multi-task accuracy as budget varies.

We extend the comparison of ATM against baseline methods across different compute budgets. Specifically, we vary the per-task finetuning epochs (K) within t and t_e and compare the average test accuracy across tasks. As shown in Figs. 4 and 7, ATM consistently outperforms the baselines, with its advantage growing as the budget increases. ATM surpasses the best baseline by 7%, 11%, and 21% for budgets of 2, 4, and 10 epochs, respectively. Detailed results for vision and NLP benchmarks can be found in Appendix B.2.

Interestingly, while ATM’s accuracy improves with more finetuning epochs, the baseline methods exhibit the opposite trend; see Fig. 6. In other words, *the more specialized the task-specific models, the*

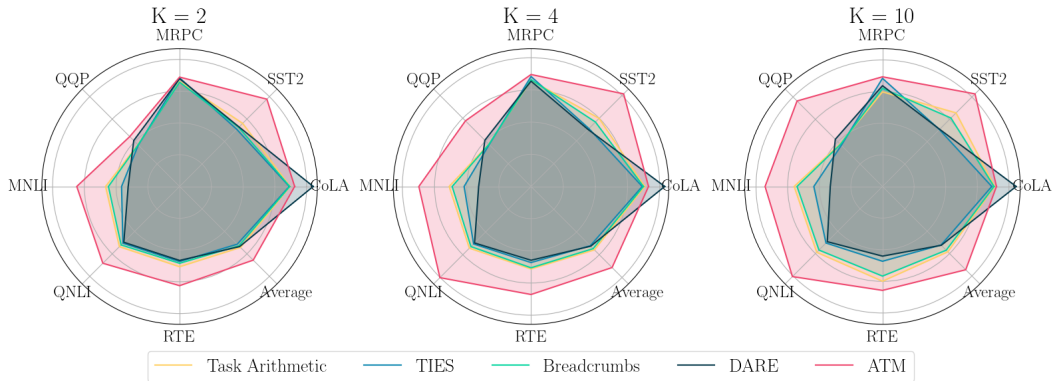


Figure 7: Comparisons as computational budget K varies for RoBERTa-base.

	CIFAR100	DTD	EuroSAT	GTSRB	MNIST	RESISC45	SVHN	Average
Task Arithmetic	0.59	0.46	0.78	0.61	0.96	0.63	0.77	0.69
TIES	0.70	0.51	0.76	0.60	0.94	0.73	0.78	0.72
Breadcrumbs	0.60	0.47	0.77	0.60	0.95	0.63	0.75	0.68
<i>valFT ATM: 10 Orders</i>	0.78	0.61	0.53	0.97	0.99	0.88	0.95	0.82
<i>ATM: 10 Orders</i>	0.79	0.61	0.98	0.97	0.99	0.89	0.96	0.89
<i>ATM: 30 Orders</i>	0.83	0.68	0.99	0.99	1.00	0.94	0.97	0.91

Table 1: Accuracy comparison under original baseline settings (ViT-B-16).

lower the performance of the unified multi-task model. ATM avoids this issue by gradually specializing the intermediate multi-task models.

6.4 COMPARISONS IN ORIGINAL SETTINGS

Given the available training data, we compare three ATM settings against various baselines under their original settings: (i) *ATM* finetuned on validation data (*valFT ATM*) for 10 iterations of 1 epoch, (ii) *ATM* finetuned on training data for 10 iterations of 1 epoch, and (iii) *ATM* finetuned on training data to convergence for 30 iterations of 1 epoch. As illustrated in Table 1, all *ATM* variants significantly outperform the baselines. With a 10-epoch budget and available training data, ATM achieves an average accuracy of 89%, leading by 17% over the best-performing baseline. Without compute restrictions, ATM converges after 30 iterations, achieving a remarkable accuracy of 91%.

6.5 TRAINING-DATA FREE SETTING

A common realistic constraint is the lack of per-task training data, as finetuned models are often sourced from online repositories. In this section, we assume only the availability of validation data, typically used by baselines for hyperparameter tuning. Unlike the baselines, ATM uses this validation data for finetuning the tasks, leaving hyperparameters untuned.

We define this variant as *valFT ATM* and compare its performance against standard *ATM* and the baselines, using author-recommended hyperparameters for fair comparisons. As presented in Table 1, *valFT ATM* outperforms the best baseline by 10%. While the 7% gap between *valFT ATM* and *ATM* is due to the limited finetuning data, *valFT ATM* performs comparably to *ATM* on all tasks except *EuroSAT*. A similar trend is observed on the NLP benchmark.

7 DISCUSSION

7.1 ORTHOGONALITY

Orthogonality between task vectors has been recommended as a desirable property for multi-task merging (Ilharco et al., 2022). Davari & Belilovsky (2023) adopt pairwise cosine similarity between

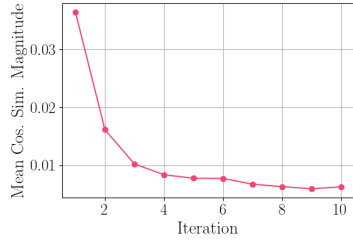


Figure 9: Average magnitudes of pairwise cosine similarity between ATM task vectors.

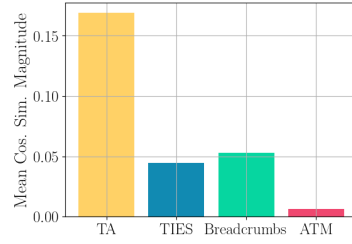


Figure 10: Average magnitudes of cosine similarity between task vectors.

task vectors as a proxy for task interference. Following this line, we again back the validity of this observation by identifying a positive correlation between ATM performance and task vector orthogonality. Fig. 9 highlights that as the number of ATM iterations increases, the magnitude of cosine similarity between task vectors tends to shrink, suggesting greater orthogonality as performance improves. Furthermore, as depicted in Fig. 10, we find that ATM task vectors exhibit lower-magnitude average cosine similarity compared to the baseline methods.

7.2 TASK PROFICIENCY IS NOT MERGEABILITY

As supported by figures 6 and 2, task-specific expertise does not imply multi-task performance. We observe that better-performing task-specific models result in worse multi-task models when adopting baseline methods, hinting that *downstream performance is not a predictor of post-merging performance*. We speculate that specialized models end up in highly dispersed locations in the parameter space, and merging them abruptly in a one-shot fashion generates a suboptimal multi-task model; this can be observed in Fig. 8, where baseline methods end up all in the same (suboptimal) loss basin. From the perspective of gradient approximation, this degradation can be explained by the fact that vanilla task vectors approximate increasingly noisy multi-task gradients when finetuning occurs for multiple epochs. On the contrary, a lower degree of specialization ensures the task-specific models remain closer to the pretrained checkpoint in the parameter space, as evinced by Ortiz-Jimenez et al. (2024) from the perspective of weight disentanglement in the tangent space, thus leading to less aggressive updates when merging. The above insights translate to less aggressive updates (shorter-norm task vectors) being more amenable to merging. This phenomenon is also consistent with the findings of Lu et al. (2024), explaining this phenomenon by the vanquishing common knowledge due to task-specific finetuning. Again, in view of gradient approximation, fewer epochs of finetuning yields a better approximation of the multi-task gradient, with a single epoch achieving the best approximation. Hence, our theoretical explanation generalizes the previous observations on this phenomenon. Capitalizing on this, ATM gradually aggregates task-specific models and updates the base model accordingly, merging less aggressively but over multiple iterations. At each iteration, the ATM task vectors represent the best nudges for the current base model without referring back to the initial pretrained model as all baseline methods do.

7.3 EDUCATED TRAJECTORY

Task arithmetic performs the aggregation step abruptly in a one-shot fashion over the initial pretrained checkpoint, likely overshooting the multi-task optimum. In ATM, however, the loss landscape is traversed iteration by iteration as the base model updates, leading to more informed nudges toward the multi-task optimum. Fig. 8 depicts the 2D projection of various checkpoints via PCA. Notably, TIES and breadcrumbs, being post-hoc enhancements of task arithmetic, end up around the same basin, whereas ATM takes gradual steps toward a different and better basin, signaling the effectiveness of our novel iterative merging paradigm.

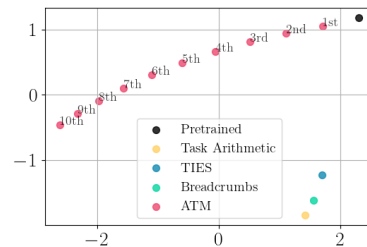


Figure 8: 2D PCA projection of various approaches.

7.4 TIME AND MEMORY COMPLEXITIES

We compare ATM to the baselines in terms of time and memory consumption, assuming the backbone has d parameters. Memory-wise, ATM has no additional requirements compared to task arithmetic, as task vectors can be deleted after each merge step. The time complexity of iteration- k ATM is equivalent to performing task arithmetic k times, as it involves k rounds of finetuning and merging. This time complexity is generally negligible compared to TIES and breadcrumbs, whose dominant overhead originates from pruning task vectors post-hoc according to the magnitude ranking of all weights, with a time complexity of $O(d * \log(d))$. As outlined in Table 2, ATM is faster than TIES and breadcrumbs as long as $\log(d)$ is asymptotically greater than k , which is typically the case since k is usually a small constant (e.g., 10).

Method	Time	Memory
Task Arithmetic	$O(n * d)$	$O(d)$
TIES	$O(n * d * \log(d))$	$O(d)$
Breadcrumbs	$O(n * d * \log(d))$	$O(d)$
ATM	$O(k * n * d)$	$O(d)$

Table 2: Comparison of methods in terms of time and memory complexity.

7.5 LIMITATIONS OF ITERATIVE MERGING

While we have demonstrated the benefits of ATM in various settings, its iterative nature has some drawbacks. Specifically, iterative merging does not immediately provide a task representation for new tasks, as it produces a series of K vectors per task. However, it remains the best approach for obtaining a single model that performs well across all tasks. We ensured a fair comparison by using the same compute budget and data requirements, showing that a small validation set suffices for effective use of the framework – this is standard in the literature, typically used for hyperparameter optimization. Lastly, although ATM resembles gradient descent on the union of tasks, it retains a key advantage of task arithmetic: by generating task vectors independently, it avoids centralizing data, making it suitable for federated settings where data privacy is critical.

8 CONCLUSIONS

In conclusion, this paper identifies a key limitation of task arithmetic – overshooting due to abrupt model merging – and establishes its connection to gradient descent, forming the basis for our proposed model merging framework. We present Alternating Tuning and Merging (ATM), an iterative framework that addresses the shortcomings of one-shot merging techniques. By alternating between finetuning and merging, ATM effectively prevents overshooting and enhances multi-task performance. Extensive experiments on computer vision and NLP benchmarks demonstrate that ATM achieves state-of-the-art accuracy while maintaining computational efficiency comparable to existing baselines. We explain the effectiveness of ATM from the perspective of multi-task gradient approximation. Additionally, our theoretical analysis reveals that ATM optimizes the upper bound of the loss over the union of all the tasks and improves task vector orthogonality. The flexibility of ATM opens numerous future research directions, including the integration of interference-mitigation techniques and further refinements through advancements from the gradient descent literature.

ETHICS STATEMENT

This research was conducted with a strong commitment to ethical standards in both data usage and experimental methodology. All datasets utilized in this study are publicly available. No personally identifiable information was accessed or used during the course of this research. Additionally, the experiments were designed to ensure fair comparisons across methods. We encourage future work that adheres to these same principles and addresses the broader societal impacts of machine learning.

REPRODUCIBILITY STATEMENT

We are committed to ensuring the reproducibility of our results and have taken steps to facilitate this for the broader research community. The code, datasets, and configurations used for the experiments in this paper are made available via a public repository. We are open to providing further instructions on the usage of our code. The hyperparameters, frameworks, and evaluation metrics have been

thoroughly documented, and we provide clear descriptions of our experimental setup to allow for straightforward replication of our findings. We encourage the community to utilize these resources and provide feedback for further improvements.

ACKNOWLEDGMENTS

This work is supported by the ERC grant no.802554 (SPECGEO), PRIN 2020 project no.2020TA3K9N (LEGO.AI), and PNRR MUR project PE0000013-FAIR.

REFERENCES

- Samuel Ainsworth, Jonathan Hayase, and Siddhartha Srinivasa. Git Re-Basin: Merging models modulo permutation symmetries. In *The Eleventh International Conference on Learning Representations*, 2022.
- Gong Cheng, Junwei Han, and Xiaoqiang Lu. Remote sensing image scene classification: Benchmark and state of the art. *Proceedings of the IEEE*, 105(10), 2017.
- Leshem Choshen, Elad Venezian, Noam Slonim, and Yoav Katz. Fusing finetuned models for better pretraining. *ArXiv preprint*, abs/2204.03044, 2022. URL <https://arxiv.org/abs/2204.03044>.
- Mircea Cimpoi, Subhransu Maji, Iasonas Kokkinos, Sammy Mohamed, and Andrea Vedaldi. Describing textures in the wild. In *2014 IEEE Conference on Computer Vision and Pattern Recognition, CVPR 2014, Columbus, OH, USA, June 23-28, 2014*. IEEE Computer Society, 2014. doi: 10.1109/CVPR.2014.461. URL <https://doi.org/10.1109/CVPR.2014.461>.
- Donato Crisostomi, Marco Fumero, Daniele Baieri, Florian Bernard, and Emanuele Rodolà. c^2m^3 : Cycle-consistent multi-model merging. In *Advances in Neural Information Processing Systems*, volume 37, 2024.
- Nico Daheim, Thomas Möllenhoff, Edoardo Ponti, Iryna Gurevych, and Mohammad Emtiyaz Khan. Model merging by uncertainty-based gradient matching. In *Proc. ICLR*, 2023.
- MohammadReza Davari and Eugene Belilovsky. Model breadcrumbs: Scaling multi-task model merging with sparse masks. *ArXiv preprint*, abs/2312.06795, 2023. URL <https://arxiv.org/abs/2312.06795>.
- Pala Tej Deep, Rishabh Bhardwaj, and Soujanya Poria. Della-merging: Reducing interference in model merging through magnitude-based sampling. *ArXiv preprint*, abs/2406.11617, 2024. URL <https://arxiv.org/abs/2406.11617>.
- Jacob Devlin, Ming-Wei Chang, Kenton Lee, and Kristina Toutanova. BERT: Pre-training of deep bidirectional transformers for language understanding. In *Proceedings of the 2019 Conference of the North American Chapter of the Association for Computational Linguistics: Human Language Technologies, Volume 1 (Long and Short Papers)*. Association for Computational Linguistics, 2019. doi: 10.18653/v1/N19-1423. URL <https://aclanthology.org/N19-1423>.
- Alexey Dosovitskiy, Lucas Beyer, Alexander Kolesnikov, Dirk Weissenborn, Xiaohua Zhai, Thomas Unterthiner, Mostafa Dehghani, Matthias Minderer, Georg Heigold, Sylvain Gelly, Jakob Uszkoreit, and Neil Houlsby. An image is worth 16x16 words: Transformers for image recognition at scale. In *9th International Conference on Learning Representations, ICLR 2021, Virtual Event, Austria, May 3-7, 2021*. OpenReview.net, 2021. URL <https://openreview.net/forum?id=YicbFdNTTy>.
- Rahim Entezari, Hanie Sedghi, Olga Saukh, and Behnam Neyshabur. The role of permutation invariance in linear mode connectivity of neural networks. In *The Tenth International Conference on Learning Representations, ICLR 2022, Virtual Event, April 25-29, 2022*. OpenReview.net, 2022. URL <https://openreview.net/forum?id=dNigytemkL>.

-
- Jonathan Frankle, Gintare Karolina Dziugaite, Daniel Roy, and Michael Carbin. Linear mode connectivity and the lottery ticket hypothesis. In *Proceedings of the 37th International Conference on Machine Learning, ICML 2020, 13-18 July 2020, Virtual Event*, volume 119 of *Proceedings of Machine Learning Research*. PMLR, 2020. URL <http://proceedings.mlr.press/v119/frankle20a.html>.
- Patrick Helber, Benjamin Bischke, Andreas Dengel, and Damian Borth. Eurosat: A novel dataset and deep learning benchmark for land use and land cover classification. *IEEE Journal of Selected Topics in Applied Earth Observations and Remote Sensing*, 12(7), 2019.
- Sebastian Houben, Johannes Stallkamp, Jan Salmen, Marc Schlipsing, and Christian Igel. Detection of traffic signs in real-world images: The German Traffic Sign Detection Benchmark. In *International Joint Conference on Neural Networks*, number 1288, 2013.
- Chenyu Huang, Peng Ye, Tao Chen, Tong He, Xiangyu Yue, and Wanli Ouyang. Emr-merging: Tuning-free high-performance model merging. *ArXiv preprint*, abs/2405.17461, 2024. URL <https://arxiv.org/abs/2405.17461>.
- Gabriel Ilharco, Marco Tulio Ribeiro, Mitchell Wortsman, Suchin Gururangan, Ludwig Schmidt, Hannaneh Hajishirzi, and Ali Farhadi. Editing models with task arithmetic. *The Eleventh International Conference on Learning Representations*, 2022.
- Xisen Jin, Xiang Ren, Daniel Preotiuc-Pietro, and Pengxiang Cheng. Dataless knowledge fusion by merging weights of language models. *ArXiv preprint*, abs/2212.09849, 2022. URL <https://arxiv.org/abs/2212.09849>.
- Alexia Jolicoeur-Martineau, Emy Gervais, Kilian Fatras, Yan Zhang, and Simon Lacoste-Julien. Population parameter averaging (papa). *ArXiv preprint*, abs/2304.03094, 2023. URL <https://arxiv.org/abs/2304.03094>.
- Keller Jordan, Hanie Sedghi, Olga Saukh, Rahim Entezari, and Behnam Neyshabur. REPAIR: RENormalizing permuted activations for interpolation repair. In *The Eleventh International Conference on Learning Representations*, 2023.
- Alex Krizhevsky, Geoffrey Hinton, et al. Learning multiple layers of features from tiny images. 2009.
- Y. Lecun, L. Bottou, Y. Bengio, and P. Haffner. Gradient-based learning applied to document recognition. *Proceedings of the IEEE*, 86(11), 1998. doi: 10.1109/5.726791.
- Yinhan Liu. Roberta: A robustly optimized bert pretraining approach. *ArXiv preprint*, abs/1907.11692, 2019. URL <https://arxiv.org/abs/1907.11692>.
- Zhenyi Lu, Chenghao Fan, Wei Wei, Xiaoye Qu, Dangyang Chen, and Yu Cheng. Twin-merging: Dynamic integration of modular expertise in model merging. *arXiv preprint arXiv:2406.15479*, 2024.
- Michael Matena and Colin Raffel. Merging models with fisher-weighted averaging. 2021.
- Aviv Navon, Aviv Shamsian, Ethan Fetaya, Gal Chechik, Nadav Dym, and Haggai Maron. Equivariant deep weight space alignment, 2023.
- Yuval Netzer, Tao Wang, Adam Coates, Alessandro Bissacco, Baolin Wu, Andrew Y Ng, et al. Reading digits in natural images with unsupervised feature learning. In *NIPS workshop on deep learning and unsupervised feature learning*, volume 2011. Granada, 2011.
- Guillermo Ortiz-Jimenez, Alessandro Favero, and Pascal Frossard. Task arithmetic in the tangent space: krizhevsky2009learning: Improved editing of pre-trained models. *Advances in Neural Information Processing Systems*, 36, 2024.
- Ashwinee Panda, Berivan Isik, Xiangyu Qi, Sanmi Koyejo, Tsachy Weissman, and Prateek Mittal. Lottery ticket adaptation: Mitigating destructive interference in llms. *ArXiv preprint*, abs/2406.16797, 2024. URL <https://arxiv.org/abs/2406.16797>.

Sidak Pal Singh and Martin Jaggi. Model fusion via optimal transport. In Hugo Larochelle, Marc’Aurelio Ranzato, Raia Hadsell, Maria-Florina Balcan, and Hsuan-Tien Lin (eds.), *Advances in Neural Information Processing Systems 33: Annual Conference on Neural Information Processing Systems 2020, NeurIPS 2020, December 6-12, 2020, virtual*, 2020. URL <https://proceedings.neurips.cc/paper/2020/hash/fb2697869f56484404c8ceee2985b01d-Abstract.html>.

Alex Wang, Amanpreet Singh, Julian Michael, Felix Hill, Omer Levy, and Samuel R. Bowman. Glue a multi-task benchmark and analysis platform for natural language understanding. In *7th International Conference on Learning Representations, ICLR 2019, New Orleans, LA, USA, May 6-9, 2019*. OpenReview.net, 2019. URL <https://openreview.net/forum?id=rJ4km2R5t7>.

Ke Wang, Nikolaos Dimitriadis, Guillermo Ortiz-Jimenez, François Fleuret, and Pascal Frossard. Localizing task information for improved model merging and compression. In *Forty-first International Conference on Machine Learning*, 2024.

Mitchell Wortsman, Gabriel Ilharco, Samir Yitzhak Gadre, Rebecca Roelofs, Raphael Gontijo Lopes, Ari S. Morcos, Hongseok Namkoong, Ali Farhadi, Yair Carmon, Simon Kornblith, and Ludwig Schmidt. Model soups: averaging weights of multiple fine-tuned models improves accuracy without increasing inference time. In Kamalika Chaudhuri, Stefanie Jegelka, Le Song, Csaba Szepesvári, Gang Niu, and Sivan Sabato (eds.), *International Conference on Machine Learning, ICML 2022, 17-23 July 2022, Baltimore, Maryland, USA*, volume 162 of *Proceedings of Machine Learning Research*. PMLR, 2022. URL <https://proceedings.mlr.press/v162/wortsman22a.html>.

Prateek Yadav, Derek Tam, Leshem Choshen, Colin Raffel, and Mohit Bansal. Ties-merging: Resolving interference when merging models. 2023.

Enneng Yang, Zhenyi Wang, Li Shen, Shiwei Liu, Guibing Guo, Xingwei Wang, and Dacheng Tao. Adamerging: Adaptive model merging for multi-task learning. In *The Twelfth International Conference on Learning Representations*, 2023.

Enneng Yang, Li Shen, Zhenyi Wang, Guibing Guo, Xiaojun Chen, Xingwei Wang, and Dacheng Tao. Representation surgery for multi-task model merging. *ArXiv preprint*, abs/2402.02705, 2024. URL <https://arxiv.org/abs/2402.02705>.

Le Yu, Bowen Yu, Haiyang Yu, Fei Huang, and Yongbin Li. Language models are super mario: Absorbing abilities from homologous models as a free lunch. In *Forty-first International Conference on Machine Learning*, 2023.

A PROOFS

A.1 PROOFS OF THEOREM 3.1 AND COROLLARY 3.1.1

In this section, we provide proofs for Theorem 3.1 and Corollary 3.1.1. For clarity, we restate both the theorem and corollary.

Theorem. Let $\{\theta_t^{(k)}\}_{t=1}^{|T|}$ be a set of models obtained by finetuning the base model θ_{base} for k epochs on tasks T using GD with a learning rate η , where finetuning task $t \in T$ minimizes the loss $\bar{L}_t(\theta) = \frac{1}{n_t} \sum_{i=1}^{n_t} \ell(x_i, y_i, \theta)$. Additionally, let $\{\tau_t^{(k)}\}_{t=1}^{|T|}$ denote the corresponding set of task vectors, with each $\tau_t^{(k)} = \theta_t^{(k)} - \theta_{base}$. Let $\tau_{MT}^{(k)}$ be the multi-task vector $\tau_{MT}^{(k)} = \sum_{t \in T} \tau_t^{(k)}$. Finally, let $\theta_{MT}^{(k)}$ represent the model obtained by minimizing the combined loss $\sum_{i=1}^{|T|} \bar{L}_i$ for k epochs using

GD with a learning rate of $\alpha\eta$. It holds that

$$\tau_{MT}^{(1)} = -\eta \nabla \sum_{t \in T} \bar{L}_t(\theta_{base}) \quad (10)$$

$$\tau_{MT}^{(k)} = -\eta \sum_{t \in T} \sum_{j=0}^{k-1} \nabla \bar{L}_i(\theta_{MT}^{(j)}) + \frac{\eta^2}{2} C(\{\theta_{MT}^{(j)}\}_{j=1}^{k-2}) + O(\eta^3) \quad (11)$$

with

$$C(\{\theta_{MT}^{(j)}\}_{j=1}^h) = \sum_{t \in T} \sum_{\ell=0}^h \nabla^2 \bar{L}_t(\theta_{MT}^{(\ell)}) \sum_{m=0}^{\ell} \left[\alpha \sum_{t' \neq t, t' \in T} \nabla \bar{L}'_t(\theta_{MT}^{(m)}) + (\alpha - 1) \nabla \bar{L}_t(\theta_{MT}^{(m)}) \right] \quad (12)$$

Corollary. Let $\theta_{TA}^{(k)} = \theta_{base} + \alpha \sum_{t=1}^T \tau_t^{(k)}$ be the model obtained using vanilla task arithmetics. Using the same notation of Theorem 3.1, it holds that

$$\theta_{TA}^{(1)} = \theta_{MT}^{(1)} \quad (13)$$

$$\theta_{TA}^{(k)} = \theta_{MT}^{(k)} + \frac{\eta^2}{2} C(\{\theta_{MT}^{(j)}\}_{j=1}^{k-2}) + O(\eta^3) \quad \text{for } k > 1 \quad (14)$$

We recall that $\theta_i^{(k)}$ is the model obtained by finetuning on task i for k epochs, and that both the finetuning on different tasks and the training on the average loss start from a pretrained model θ_{base} .

To prove the statement of the theorem and of the corollary we need a intermediate result. We introduce the following notation:

$$r_i(\theta) = \alpha \sum_{j \neq i} \nabla \bar{L}_j(\theta) + (\alpha - 1) \nabla \bar{L}_i(\theta) = \alpha \sum_{j=1}^{|T|} \nabla \bar{L}_j(\theta) - \nabla \bar{L}_i(\theta_{base}) \quad (15)$$

$$p_i^k(\theta_{base}, \theta_{MT}^{(1)}, \dots, \theta_{MT}^{(k)}) = \sum_{j=0}^k r_i(\theta_{MT}^{(j)}) \quad (16)$$

$$s_i^k(\theta_{base}, \dots, \theta_{MT}^{(k)}) = \sum_{j=0}^k \nabla^2 \bar{L}_i(\theta_{MT}^{(j)}) [p_i^j(\theta_{base}, \dots, \theta_{MT}^{(j-1)})]. \quad (17)$$

Lemma A.1. Using the notation introduced in Theorem 3.1, it holds that

$$\theta_i^{(1)} = \theta_{MT}^{(1)} + \eta p_i^0(\theta_{base}) \quad (18)$$

and for $m \geq 2$

$$\theta_i^{(m+1)} = \theta_{MT}^{(m+1)} + \eta p_i^m(\theta_{base}, \dots, \theta_{MT}^{(m)}) - \frac{\eta^2}{2} s_i^{m-1}(\theta_{base}, \dots, \theta_{MT}^{(m-1)}) + O(\eta^3) \quad (19)$$

Proof. We first show that the statement is true for $m = 1$, and then prove the results for $m \geq 2$ by induction. In this case, the base case is given for $m = 2$. In the induction step, instead, we prove that if the statement holds for any given case m then it must also hold for the next case $m + 1$.

$m = 1$. First epoch For each task $i = 1, \dots, |T|$

$$\theta_i^{(1)} = \theta_{base} - \eta \nabla \bar{L}_i(\theta_{base}) \quad \text{while} \quad \theta_{MT}^{(1)} = \theta_{base} - \alpha \eta \sum_{i \in T} \nabla \bar{L}_i(\theta_{base}).$$

Consequently, it holds that

$$\begin{aligned} \theta_i^1 &= \theta_{MT}^{(1)} + \eta \left[\alpha \sum_{j \neq i} \nabla \bar{L}_j(\theta_{base}) + (\alpha - 1) \nabla \bar{L}_i(\theta_{base}) \right] \\ &= \theta_{MT}^{(1)} + \eta r_i(\theta_{base}) = \theta_{MT}^{(1)} + \eta p_i^0(\theta_{base}). \end{aligned}$$

$m = 2$. **Second epoch**

$$\begin{aligned}
\theta_i^{(2)} &= \theta_i^{(1)} - \eta \nabla \bar{L}_i(\theta_i^{(1)}) \\
&= \theta_{\text{MT}}^{(1)} + \eta r_i(\theta_{\text{base}}) - \eta \nabla \bar{L}_i \left(\theta_{\text{MT}}^{(1)} + \eta r_i(\theta_{\text{base}}) \right) \\
&\stackrel{\text{Taylor}}{\approx} \theta_{\text{MT}}^{(1)} + \eta r_i(\theta_{\text{base}}) - \eta \nabla \bar{L}_i(\theta_{\text{MT}}^{(1)}) - \frac{\eta^2}{2} \nabla^2 \bar{L}_i(\theta_{\text{MT}}^{(1)}) r_i(\theta_{\text{base}}) + O(\eta^3) \\
&= \theta_{\text{MT}}^{(1)} - \eta \nabla \bar{L}_i(\theta_{\text{MT}}^{(1)}) + \eta r_i(\theta_{\text{base}}) - \frac{\eta^2}{2} \nabla^2 \bar{L}_i(\theta_{\text{MT}}^{(1)}) r_i(\theta_{\text{base}}) + O(\eta^3) \\
&= \theta_{\text{MT}}^{(1)} - \eta \nabla \bar{L}_i(\theta_{\text{MT}}^{(1)}) + \eta \alpha \sum_{t \in T} \nabla \bar{L}_i(\theta_{\text{MT}}^{(1)}) - \eta \alpha \sum_{t \in T} \nabla \bar{L}_i(\theta_{\text{MT}}^{(1)}) + \eta r_i(\theta_{\text{base}}) \\
&\quad - \frac{\eta^2}{2} \nabla^2 \bar{L}_i(\theta_{\text{MT}}^{(1)}) r_i(\theta_{\text{base}}) + O(\eta^3) \\
&= \theta_{\text{MT}}^{(1)} + \eta r_i(\theta_{\text{MT}}^{(1)}) + \eta r_i(\theta_{\text{base}}) - \frac{\eta^2}{2} \nabla^2 \bar{L}_i(\theta_{\text{MT}}^{(1)}) r_i(\theta_{\text{base}}) + O(\eta^3) \\
&= \theta_{\text{MT}}^1 + \eta p_i^1(\theta_{\text{base}}, \dots, \theta_{\text{MT}}^{(1)}) - \frac{\eta^2}{2} s_i^0(\theta_{\text{base}}) + O(\eta^3)
\end{aligned}$$

Inductive step Let us assume that

$$\theta_i^{(m)} = \theta_{\text{MT}}^{(m)} + \eta p_i^{m-1}(\theta_{\text{base}}, \dots, \theta_{\text{MT}}^{(m-1)}) - \frac{\eta^2}{2} s_i^{m-2}(\theta_{\text{base}}, \dots, \theta_{\text{MT}}^{(m-2)}) + O(\eta^3)$$

We can derive that

$$\begin{aligned}
\theta_i^{(m+1)} &= \theta_i^{(m)} - \eta \nabla \bar{L}_i(\theta_i^{(m)}) \\
&= \theta_{\text{MT}}^{(m)} + \eta p_i^{m-1}(\theta_{\text{base}}, \dots, \theta_{\text{MT}}^{(m-1)}) - \frac{\eta^2}{2} s_i^{m-2}(\theta_{\text{base}}, \dots, \theta_{\text{MT}}^{(m-2)}) - \eta \nabla \bar{L}_i(\theta_i^{(m)}) + O(\eta^3) \\
&= \theta_{\text{MT}}^{(m)} + \eta p_i^{m-1}(\theta_{\text{base}}, \dots, \theta_{\text{MT}}^{(m-1)}) - \frac{\eta^2}{2} s_i^{m-2}(\theta_{\text{base}}, \dots, \theta_{\text{MT}}^{(m-2)}) \\
&\quad - \eta \nabla \bar{L}_i \left(\theta_{\text{MT}}^{(m)} + \eta p_i^{m-1}(\theta_{\text{base}}, \dots, \theta_{\text{MT}}^{(m-1)}) - \frac{\eta^2}{2} s_i^{m-2}(\theta_{\text{base}}, \dots, \theta_{\text{MT}}^{(m-2)}) \right) + O(\eta^3) \\
&= \theta_{\text{MT}}^{(m)} + \eta p_i^{m-1}(\theta_{\text{base}}, \dots, \theta_{\text{MT}}^{(m-1)}) - \frac{\eta^2}{2} s_i^{m-2}(\theta_{\text{base}}, \dots, \theta_{\text{MT}}^{(m-2)}) \\
&\quad - \eta \nabla \bar{L}_i(\theta_{\text{MT}}^{(m)}) - \frac{\eta}{2} \nabla^2 \bar{L}_i(\theta_{\text{MT}}^{(m)}) \left(\eta p_i^{m-1}(\theta_{\text{base}}, \dots, \theta_{\text{MT}}^{(m-1)}) - \frac{\eta^2}{2} s_i^{m-2}(\theta_{\text{base}}, \dots, \theta_{\text{MT}}^{(m-2)}) \right) + O(\eta^3) \\
&= \theta_{\text{MT}}^{(m)} + \eta p_i^{m-1}(\theta_{\text{base}}, \dots, \theta_{\text{MT}}^{(m-1)}) - \frac{\eta^2}{2} s_i^{m-2}(\theta_{\text{base}}, \dots, \theta_{\text{MT}}^{(m-2)}) \\
&\quad - \eta \nabla \bar{L}_i(\theta_{\text{MT}}^{(m)}) - \frac{\eta^2}{2} \nabla^2 \bar{L}_i(\theta_{\text{MT}}^{(m)}) p_i^{m-1}(\theta_{\text{base}}, \dots, \theta_{\text{MT}}^{(m-1)}) + O(\eta^3) \\
&= \theta_{\text{MT}}^{(m+1)} + \eta p_i^m(\theta_{\text{base}}, \dots, \theta_{\text{MT}}^{(m)}) - \frac{\eta^2}{2} s_i^{m-1}(\theta_{\text{base}}, \dots, \theta_{\text{MT}}^{(m-1)}) + O(\eta^3)
\end{aligned}$$

□

Proof Theorem and Corollary. For the first epoch

$$\theta_{\text{TA}}^{(1)} = \theta_{\text{base}} + \alpha \sum_{i \in T} \tau_i^{(1)} = \theta_{\text{base}} - \eta \alpha \sum_{i \in T} \nabla \bar{L}_i(\theta_{\text{base}})$$

while, choosing $\alpha \eta$ as learning rate for the loss $\sum_{i \in T} \bar{L}_i$:

$$\theta_{\text{MT}}^{(1)} = \theta_{\text{base}} - \alpha \eta \sum_{i \in T} \nabla \bar{L}_i(\theta_{\text{base}}).$$

So $\theta_{\text{MT}}^{(1)} = \theta_{\text{TA}}^{(1)}$.

For $k \geq 2$, notice that

$$\theta_{\text{MT}}^{(k)} = \theta_{\text{base}} - \alpha\eta \sum_{j=0}^{k-1} \nabla \sum_{t \in T} \bar{L}_i(\theta_{\text{MT}}^{(j)}). \quad (20)$$

Now, using Lemma A.1, we get:

$$\begin{aligned} & -\alpha\eta \sum_{j=0}^{k-1} \nabla \sum_{t \in T} \bar{L}_i(\theta_{\text{MT}}^{(j)}) + \eta p_i^{k-1}(\eta^0, \dots, \eta_{\text{MT}}^{k-1}) \\ &= -\alpha\eta \sum_{j=0}^{k-1} \nabla \sum_{t \in T} \bar{L}_i(\theta_{\text{MT}}^{(j)}) + \sum_{j=0}^{k-1} r_i(\theta_{\text{MT}}^{(j)}) \\ &= -\alpha\eta \sum_{j=0}^{k-1} \nabla \sum_{t \in T} \bar{L}_i(\theta_{\text{MT}}^{(j)}) + \sum_{j=0}^{k-1} \alpha \sum_{j \in T} \nabla \bar{L}_j(\theta_{\text{MT}}^{(j)}) - \nabla \bar{L}_i(\theta_{\text{MT}}^{(j)}) \\ &= -\eta \sum_{j=0}^{k-1} \nabla \bar{L}_i(\theta_{\text{MT}}^{(j)}). \end{aligned}$$

Namely:

$$\begin{aligned} \theta_i^{(m+1)} &= \theta_{\text{MT}}^{(m+1)} + \eta p_i^m(\theta_{\text{base}}, \dots, \theta_{\text{MT}}^{(m)}) - \frac{\eta^2}{2} s_i^{m-1}(\theta_{\text{base}}, \dots, \theta_{\text{MT}}^{(m-1)}) + O(\eta^3) \\ &= \theta_{\text{base}} - \alpha\eta \sum_{j=0}^m \nabla \sum_{t \in T} \bar{L}_i(\theta_{\text{MT}}^{(j)}) + \eta p_i^m(\theta_{\text{base}}, \dots, \theta_{\text{MT}}^{(m)}) - \frac{\eta^2}{2} s_i^{m-1}(\theta_{\text{base}}, \dots, \theta_{\text{MT}}^{(m-1)}) + O(\eta^3) \\ &= \theta_{\text{base}} - \eta \sum_{j=0}^m \nabla \bar{L}_i(\theta_{\text{MT}}^{(j)}) - \frac{\eta^2}{2} s_i^{m-1}(\theta_{\text{base}}, \dots, \theta_{\text{MT}}^{(m-1)}) + O(\eta^3) \end{aligned}$$

we can rewrite the tasks vectors as

$$\tau_i^{(k)} = \theta_i^{(k)} - \theta_{\text{base}} \quad (21)$$

$$= -\eta \sum_{j=0}^{k-1} \nabla \bar{L}_i(\theta_{\text{MT}}^{(j)}) - \frac{\eta^2}{2} s_i^{k-2}(\theta_{\text{base}}, \dots, \theta_{\text{MT}}^{(k-2)}) + O(\eta^3) \quad (22)$$

Consequently the model obtained with TA is

$$\begin{aligned} \theta_{\text{TA}}^{(k)} &= \theta_{\text{base}} + \alpha \sum_{i \in T} \tau_i^{(k)} \\ &= \theta_{\text{base}} - \eta\alpha \sum_{j=0}^{k-1} \sum_{i \in T} \nabla \bar{L}_i(\theta_{\text{MT}}^{(j)}) - \alpha \sum_{i \in T} \frac{\eta^2}{2} s_i^{k-2}(\theta_{\text{base}}, \dots, \theta_{\text{MT}}^{(k-2)}) + O(\eta^3) \\ &= \theta_{\text{MT}}^{(k)} - \alpha \sum_{i \in T} \frac{\eta^2}{2} s_i^{k-2}(\theta_{\text{base}}, \dots, \theta_{\text{MT}}^{(k-2)}) + O(\eta^3). \end{aligned}$$

□

A.2 PROOF OF THEOREM 5.1

In this section, we provide a rigorous proof of Theorem 5.1, establishing the conditions under which ATM implicitly optimizes the loss of the model trained on the union of datasets.

Proof. Suppose that when transitioning from parameters $\theta^{(i)}$ to parameters $\theta^{(i+1)}$, the change in the average loss for each dataset D_k is given by $\Delta \bar{L}_k = \bar{L}_k(\theta^{(i)}) - \bar{L}_k(\theta^{(i+1)})$. We denote by P the set of tasks for which the delta of the loss is positive and by N the set for which it is negative, namely $P = \{k \in T \text{ s.t. } \Delta \bar{L}_k > 0\}$ and $N = \{k \in T \text{ s.t. } \Delta \bar{L}_k \leq 0\}$. The set $\{1, \dots, n\} = P \cup N$. In the following formulas we will use the symbol $|\cdot|$ for different purposes. For sets, like D_i , $|D_i|$ denotes the cardinality of the set, while for scalars, such as $\Delta \bar{L}_k$, $|\Delta \bar{L}_k|$ denotes their absolute value. Since the tasks in N have negative $\Delta \bar{L}_k$, it holds that

$$\sum_{j \in N} |D_j| \Delta \bar{L}_j = - \sum_{j \in N} |D_j| |\Delta \bar{L}_j|.$$

Under the hypothesis that $\Delta L_{\text{ATM}} > \delta$, this implies $\sum_{j=1}^n \Delta_j > n\delta$. We have that $\sum_{j \in P} \Delta \bar{L}_j + \sum_{j \in N} \Delta \bar{L}_j = \sum_{j \in P} \Delta \bar{L}_j - \sum_{j \in N} |\Delta \bar{L}_j| > n\delta$, namely $\sum_{j \in P} \Delta \bar{L}_j > n\delta + \sum_{j \in N} |\Delta \bar{L}_j|$.

We want to prove that $\Delta L_{\text{target}} > 0$. Let us now consider $\Delta L_{\text{target}} > 0$ iff $\sum_{j=1}^n |D_j| \Delta_j > 0$.

$$\begin{aligned} \sum_{j=1}^n |D_j| \Delta_j &= \sum_{j \in P} |D_j| \Delta \bar{L}_j + \sum_{j \in N} |D_j| \Delta \bar{L}_j \\ &= \sum_{j \in P} |D_j| \Delta \bar{L}_j - \sum_{j \in N} |D_j| |\Delta \bar{L}_j| \\ &> \min_{j \in P} |D_j| \sum_{j \in P} \Delta \bar{L}_j - \max_{j \in N} |D_j| \sum_{j \in N} |\Delta \bar{L}_j| \\ &> \min_{j \in P} |D_j| \left[n\delta + \sum_{j \in N} |\Delta \bar{L}_j| \right] - \max_{j \in N} |D_j| \sum_{j \in N} |\Delta \bar{L}_j| \\ &= n \min_{j \in P} |D_j| \delta + \left(\min_{j \in P} |D_j| - \max_{j \in N} |D_j| \right) \sum_{j \in N} |\Delta \bar{L}_j|. \end{aligned}$$

The last line of the previous equation is positive by hypothesis, since we assumed $\delta > \frac{1}{n} \left(1 - \frac{\min_{j \in N} |D_j|}{\max_{j \in P} |D_j|} \right) \sum_{j \in N} |\Delta \bar{L}_j|$. \square

B ADDITIONAL RESULTS

B.1 FULL RESULTS OVER VARYING COMPUTATIONAL BUDGET

In the main paper, we pictorially illustrated the multi-task accuracy of the baselines and ATM variants, in the form of radar plots. For deeper analysis, here we report the full results of ATM compared to the baselines, as the computational budget varies for 2, 4, 7, and 10 epochs. See Tables 3, 4, and 5 respectively.

B.2 COSINE SIMILARITY OF EPOCH-WISE GRADIENTS

We report in Fig. 11 the cosine similarity of gradients for the first 10 epochs over DTD and EuroSAT, as these do not have a marked difference in gradient norms between the first epoch and the remaining ones in Fig. 3a. We see that the alignment of subsequent gradients observed in RESISC45 still holds in DTD, even if with less marked similarities. On the other hand, this does not seem to hold for EuroSAT.

		CIFAR100	DTD	EuroSAT	GTSRB	MNIST	RESISC45	SVHN	average
$K = 2$	Task Arithmetic	0.58	0.39	0.78	0.59	0.98	0.58	0.83	0.68
	TIES	0.76	0.46	0.71	0.55	0.96	0.71	0.81	0.71
	Breadcrumbs	0.72	0.48	0.80	0.61	0.97	0.70	0.81	0.72
	ValFT ATM	0.70	0.53	0.84	0.84	0.98	0.78	0.90	0.80
	ATM	0.74	0.51	0.89	0.76	0.98	0.74	0.89	0.79
$K = 4$	Task Arithmetic	0.71	0.48	0.80	0.62	0.97	0.71	0.82	0.73
	TIES	0.75	0.45	0.69	0.56	0.97	0.69	0.84	0.70
	Breadcrumbs	0.68	0.43	0.79	0.61	0.97	0.67	0.81	0.71
	ValFT ATM	0.66	0.55	0.73	0.85	0.98	0.83	0.94	0.79
	ATM	0.75	0.55	0.95	0.90	0.99	0.82	0.94	0.84
$K = 7$	Task Arithmetic	0.67	0.44	0.79	0.62	0.97	0.67	0.83	0.71
	TIES	0.72	0.43	0.66	0.56	0.97	0.66	0.85	0.69
	Breadcrumbs	0.65	0.41	0.76	0.62	0.97	0.62	0.81	0.69
	ValFT ATM	0.75	0.62	0.66	0.96	0.99	0.85	0.96	0.83
	ATM	0.77	0.58	0.98	0.96	0.99	0.87	0.95	0.87
$K = 10$	Task Arithmetic	0.63	0.41	0.76	0.63	0.97	0.62	0.83	0.69
	TIES	0.68	0.41	0.70	0.56	0.98	0.62	0.86	0.69
	Breadcrumbs	0.60	0.40	0.78	0.58	0.98	0.59	0.81	0.68
	ValFT ATM	0.78	0.61	0.53	0.97	0.99	0.88	0.95	0.82
	ATM	0.79	0.61	0.98	0.97	0.99	0.89	0.96	0.89

Table 3: ATM vs. Baselines as budget varies (*ViT-B-16*)

		CoLA	SST2	MRPC	QQP	MNLI	QNLI	RTE	Average
$K = 2$	Task Arithmetic	0.70	0.56	0.66	0.37	0.47	0.54	0.51	0.54
	TIES	0.69	0.51	0.68	0.37	0.37	0.51	0.47	0.51
	Breadcrumbs	0.69	0.53	0.66	0.37	0.45	0.52	0.48	0.53
	DARE	0.84	0.53	0.68	0.41	0.32	0.50	0.47	0.54
	valFT ATM	0.71	0.78	0.68	0.46	0.64	0.68	0.67	0.66
$K = 4$	Task Arithmetic	0.71	0.60	0.66	0.37	0.51	0.54	0.51	0.56
	TIES	0.69	0.51	0.68	0.37	0.42	0.51	0.47	0.52
	Breadcrumbs	0.70	0.57	0.66	0.37	0.49	0.53	0.51	0.55
	DARE	0.83	0.50	0.65	0.41	0.33	0.50	0.46	0.53
	valFT ATM	0.70	0.83	0.70	0.68	0.67	0.73	0.62	0.70
$K = 7$	Task Arithmetic	0.71	0.65	0.65	0.38	0.52	0.56	0.55	0.57
	TIES	0.69	0.51	0.68	0.37	0.42	0.51	0.47	0.52
	Breadcrumbs	0.71	0.61	0.65	0.37	0.50	0.54	0.52	0.56
	DARE	0.84	0.52	0.65	0.43	0.33	0.49	0.44	0.52
	valFT ATM	0.69	0.85	0.69	0.75	0.68	0.72	0.60	0.71
$K = 10$	Task Arithmetic	0.71	0.66	0.60	0.38	0.56	0.59	0.60	0.59
	TIES	0.69	0.51	0.68	0.37	0.43	0.51	0.47	0.52
	Breadcrumbs	0.71	0.61	0.62	0.38	0.54	0.57	0.57	0.57
	DARE	0.85	0.51	0.64	0.42	0.33	0.49	0.44	0.52
	valFT ATM	0.68	0.86	0.66	0.76	0.70	0.73	0.63	0.72
$K = 10$	ATM	0.72	0.83	0.69	0.76	0.74	0.81	0.66	0.74

Table 4: ATM vs Baselines as budget varies (*RoBERTa-base*)

		CoLA	SST2	MRPC	QQP	MNLI	QNLI	RTE	Average
$K = 2$	Task Arithmetic	0.61	0.70	0.39	0.65	0.41	0.57	0.54	0.55
	TIES	0.32	0.50	0.32	0.63	0.37	0.50	0.54	0.45
	Breadcrumbs	0.60	0.68	0.39	0.65	0.40	0.57	0.54	0.55
	DARE	0.82	0.54	0.69	0.40	0.33	0.50	0.46	0.53
	ValFT ATM	0.66	0.71	0.47	0.65	0.44	0.57	0.56	0.58
	ATM	0.68	0.68	0.39	0.64	0.46	0.56	0.61	0.58
$K = 4$	Task Arithmetic	0.59	0.66	0.39	0.67	0.41	0.55	0.57	0.55
	TIES	0.32	0.50	0.32	0.63	0.38	0.51	0.53	0.46
	Breadcrumbs	0.58	0.65	0.40	0.67	0.41	0.55	0.56	0.54
	DARE	0.82	0.53	0.66	0.43	0.33	0.50	0.47	0.54
	ValFT ATM	0.67	0.75	0.47	0.70	0.54	0.64	0.62	0.62
	ATM	0.68	0.76	0.44	0.74	0.59	0.66	0.67	0.65
$K = 7$	Task Arithmetic	0.58	0.65	0.38	0.66	0.42	0.55	0.58	0.55
	TIES	0.33	0.50	0.33	0.63	0.38	0.51	0.53	0.46
	Breadcrumbs	0.58	0.65	0.38	0.66	0.41	0.55	0.59	0.55
	DARE	0.83	0.52	0.66	0.43	0.33	0.51	0.46	0.53
	ValFT ATM	0.66	0.75	0.47	0.70	0.59	0.67	0.64	0.64
	ATM	0.69	0.81	0.51	0.78	0.63	0.70	0.66	0.68
$K = 10$	Task Arithmetic	0.59	0.66	0.39	0.64	0.42	0.55	0.59	0.55
	TIES	0.35	0.51	0.34	0.64	0.38	0.51	0.53	0.47
	Breadcrumbs	0.59	0.65	0.39	0.64	0.42	0.55	0.60	0.55
	DARE	0.82	0.51	0.69	0.42	0.33	0.51	0.47	0.54
	ValFT ATM	0.66	0.73	0.50	0.71	0.59	0.69	0.63	0.64
	ATM	0.68	0.81	0.53	0.78	0.65	0.72	0.66	0.69

Table 5: ATM vs. Baselines as budget varies (*BERT-base-uncased*)

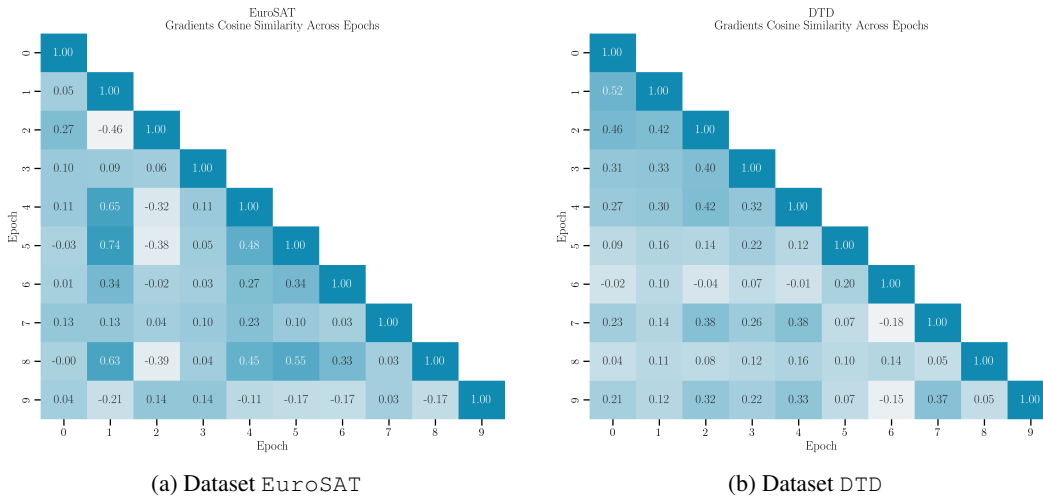


Figure 11: Pairwise cosine similarities of the gradients of the first 10 epochs over datasets that do not exhibit most of the gradient norm localized in the first epoch.